Sideband ground-state cooling of graphene with Rydberg atoms via vacuum forces

M. Miskeen Khan,[1,2,*] S. Ribeiro [ORCID],[3] J. T. Mendonça,[1,2] and H. Terças [ORCID][1,2]

[1]*Instituto Superior Técnico, Universidade de Lisboa, Portugal*
[2]*Instituto de Plasmas e Fusão Nuclear, Instituto Superior Técnico, Universidade de Lisboa, Portugal*
[3]*Joint Quantum Centre (JQC) Durham-Newcastle, Department of Physics, Durham University, United Kingdom*

We present a scheme leading to ground-state cooling of the fundamental out-of-plane (flexural) mode of a suspended graphene sheet. Our proposal exploits the coupling between a driven Rydberg atom and the graphene resonator, which is enabled by vacuum forces. Thanks to the large atomic polarizability of the Rydberg states, the Casimir-Polder force is several orders of magnitude larger than the corresponding force achieved for atoms in the ground state. By tuning the distance between the atom and the graphene membrane, we show that resolved sideband cooling is possible, bringing the occupation number of the fundamental flexural mode down to its quantum limit. Our findings are expected to motivate physical applications of graphene at extremely low temperatures.

I. INTRODUCTION

The interest around atomically thin mechanical resonators, such as graphene and other two-dimensional (2D) materials [1,2], has grown in the last years thanks to their low masses and large stiffnesses, leading to large oscillation frequencies and high-quality factors [3–6]. Those features put graphene in the run for competitive nanomechanical solutions, with a variety of important applications in quantum technology, such as storing and processing quantum information by invoking coherent coupling [7], high-precision quantum sensing [3,8–10], and quantum interferometry [11]. From the condensed-matter physics perspective, the ability to control the out-of-plane vibration of a 2D material (the so-called flexural phonon) is also very challenging because it allows for tunable control of pseudomagnetic fields [12], electron-phonon coupling [13], and selective band-gap engineering [14]. However, the quantum control of the flexural modes occurs in the near-zero thermal noise limit, where the mechanical motion is mostly due to quantum fluctuations [15]. As such, ground-state cooling of graphene resonators still preludes the applications mentioned above, and therefore an efficient, active cooling protocol is urgent. Since laser (or radiation pressure) and photothermal cooling schemes are extremely ineffective in graphene—as a result of its broadband absorption spectrum [16–20]—a possible solution could be to exploit the electromagnetic vacuum fluctuations (EVFs), emerging as a powerful resource to couple graphene resonators with a quantum emitter. Such hybrid setups offer all-optical quantum control of the membrane motion, enabling force sensing [9] and mechanical squeezing [21]. More recently, EVF has also been used for ground-state cooling of a h-BN monolayer based on electromagnetically induced transparency (EIT) [22]. Additionally, dispersion forces have a measurable effect on the levels and lifetimes of Rydberg atoms when brought close to surfaces [23,24]. However,

solutions combining the features of both vacuum forces and high-lying Rydberg states in graphene electromechanical setups are still at their infancy [25], and the possibilities offered by Rydberg states are far from being exhausted.

In this article, we describe a scheme to achieve ground-state cooling of a graphene resonator by coupling it to a Rydberg atom via vacuum forces. We exploit the large atomic polarizability of the Rydberg states and the fact that the backaction of the Casimir-Polder (CP) force depends on the atom-surface distance to construct a resolved sideband cooling protocol bringing the out-of-plane (flexural) mode down to its quantum ground state. Our findings pave the way for both quantum-technological and condensed-matter investigations for which ground-state cooling of flexural modes in suspended graphene (and eventually other 2D materials) is required.

This article is organized as follows: In Sec. II, we begin by briefly reviewing the surface-induced effects on the atomic energy states as well as on atomic decay rates, giving some numerical results for a Rydberg atom near a graphene sheet. In Sec. III, we describe the coupling mechanism between the atomic states and the flexural vibrations of a graphene membrane. Furthermore, we show that the resulting effective model allows us to operate within the resolved sideband cooling regime. The cooling process and study of the full dissipative dynamics of the system are developed in Sec. IV. We show under which conditions it is possible to achieve ground-state cooling of the graphene vibrational modes. In Sec. V, we discuss possible experimental setups for the development of our proposal. Finally, a discussion about the main results, final remarks, and discussion about future perspectives are enclosed in Sec. VI.

II. MODIFICATION OF THE ATOMIC STATES DUE TO SURFACE-SCATTERED VACUUM FLUCTUATIONS

Consider an atom placed close to a graphene membrane at a distance d along the z direction; see Fig. 1(a). The atom-surface interaction potential is calculated by assuming the
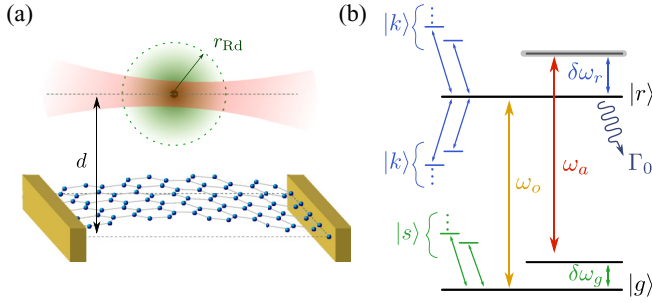
*miskeen.khan@tecnico.ulisboa.pt

FIG. 1. (a) Schematic representation of the experimental setup. A Rydberg atom is placed a distance d from a suspended graphene membrane. The out-of-plane (flexural) motion results in a modulation of the Rydberg transition frequency ω_a. (b) (not to scale) The states $|s\rangle$ contributing to the calculation of ground-state energy shift $\delta\omega_g$, lying above the energy level. For Rydberg states, the energy shift $\delta\omega_r$ accounts for contributions from both the above-and below-lying transitions $|k\rangle$. In addition, the graphene resonator induces a modification in the free-space Rydberg decay rate Γ_0.

graphene sheet to be infinitely extended, thereby neglecting possible finite-size effects. Within the formalism of macroscopic quantum electrodynamics, at zero temperature, we can write the energy shift in the ground-state $\delta\omega_g$, and total shift in the Rydberg state $\delta\omega_r$ as the sum of the nonresonant $\delta\omega_r^{\rm NR}$ and the resonant $\delta\omega_r^{\rm R}$ parts [26,27]:

$$\delta\omega_g = \frac{\hbar\mu_0}{2\pi} \int_0^\infty d\xi\,\xi^2 \alpha_g(i\xi)\,\mathrm{Tr}\,[\mathbf{G}(\mathbf{r},\mathbf{r},i\xi)], \qquad (1)$$

$$\delta\omega_r^{\rm NR} = \frac{\hbar\mu_0}{2\pi} \int_0^\infty d\xi\,\xi^2 \alpha_r(i\xi)\,\mathrm{Tr}\,[\mathbf{G}(\mathbf{r},\mathbf{r},i\xi)], \qquad (2)$$

$$\delta\omega_r^{\rm R} = -\frac{\mu_0}{3} \sum_{\ell<r} \omega_{r\ell}^2 |\mathbf{d}_{r\ell}|^2 \mathrm{Tr}\{\mathrm{Re}[\mathbf{G}(\mathbf{r},\mathbf{r},\omega_{r\ell})]\}. \qquad (3)$$

Here, $\mathbf{G}(\mathbf{r},\mathbf{r},\omega)$ is the Green tensor accounting for the relevant electromagnetic properties of graphene (refer to Appendix A for an explicit expression), $\omega_{g\ell}$ ($\omega_{r\ell}$) is the atomic transition frequency between a certain ℓ and the ground (Rydberg) states, μ_0 is the vacuum permeability, and $\mathbf{d}_{x\ell} = \langle x|\hat{\mathbf{d}}|\ell\rangle$, with $x=(g,r)$, denotes the dipole matrix elements between two states. The electromagnetic response of the atom is captured by the atomic polarizability function $\alpha_x(\omega)$,

$$\alpha_x(\omega) = \lim_{\epsilon\to 0} \frac{2}{3\hbar} \sum_\ell \frac{\omega_{x\ell}|\mathbf{d}_{x\ell}|^2}{\omega_{x\ell}^2 - \omega^2 - i\omega\epsilon}, \qquad (4)$$

where the sum is extended to all allowed atomic transitions, as depicted in Fig. 1(b).

The distance-dependent energy shift (Casimir-Polder shift) in the ground state, $\delta\omega_g$, is due to nonresonant terms ($\hat{\sigma}_{gk}\hat{a}_l^\dagger$ and $\hat{\sigma}_{kg}\hat{a}_l$) of the interaction Hamiltonian $H_{\rm int} = -\hat{\mathbf{d}} \cdot \mathbf{E}$. Here, $\hat{a}_l$ denotes the annihilation operator of the scattered electromagnetic field $\mathbf{E}$. In addition, the atomic operator $\sigma_{gk} = |g\rangle\langle k|$ describes the transitions from the ground state $|g\rangle$ to the intermediate states $|s\rangle$ (see Fig. 1). In the single-photon Hilbert space, $H_{\rm int}$ couples the polaritonic ground ($|g,0_l\rangle$) and the intermediate ($|k,1_l\rangle$) states. These excitations are followed by the re-absorption process of a photon by the atom, bringing the atom back to its ground-state (the field mode to its vacuum

state). Because these processes violate energy conservation, they are purely virtual, ensuring that the ground-state energy shift is due to nonresonant part of the interaction and its expression is given by Eq. (1). For the Rydberg state, however, the transition manifold contains both above- and below-lying states. As a result, the corresponding shift $\delta\omega_r$ contains both nonresonant and resonant terms (thus coupling the polaritonic $|r,0_l\rangle$ and $|k,1_l\rangle$ states). While the former accounts for virtual processes, the latter allow real photon transitions. The total shift $\delta\omega_r$ is then the sum of nonresonant ($\delta\omega_r^{\rm NR}$) and resonant ($\delta\omega_r^{\rm R}$) parts.

The presence of a nearby graphene surface also changes significantly the free-space spontaneous decay rate of the Rydberg state Γ_0 as

$$\Gamma = \Gamma_0 + \frac{2\mu_0}{3\hbar} \sum_{\ell<r} \omega_{r\ell}^2 |\mathbf{d}_{r\ell}|^2 \mathrm{Tr}[\mathrm{Im}[\mathbf{G}(\mathbf{r},\mathbf{r},\omega_{r\ell})]]. \qquad (5)$$

From Eqs. (1)–(5) one can observe that the amplitude of each term in the summation is given by the product of transition frequency and dipole moment magnitude of the transition involved. For the Rydberg state, the transition manifold with neighboring Rydberg states contributes with a relatively enhanced value due to the large values of the dipole-moment magnitudes. This results in the fact that energy shift and relaxation rates are much larger for Rydberg atoms than in the case of regular (non-Rydberg) atoms. This is particularly useful in the present case, where we aim to exploit the large modulation in the energy-shifting effect of the Rydberg state whenever the atom-surface distance is varied due to the out-of-plane motion of the graphene resonator. We find that, by working at a suitable atom-surface distance, the conditions for resolved sideband cooling (to be described below) are met, a demanding task which has been lacking for graphene resonators so far.

Temperature contribution

In this work, the cooling protocol could be performed at cryogenic temperatures (as low as $T=30$ mK) so thermal excitations might not play an important role. As such, we will assume the validity of the zero-temperature limit of Eqs. (1)–(5). However, this approximation is not obvious, so we will discuss it in more detail.

At finite temperatures, for an atomic state $|x\rangle$, the frequency integral in the nonresonant contributions to the energy shifts read [26]

$$\delta\omega_x^{\rm NR} = \mu_0 k_B T \sum_{j=0}^\infty {}' \xi_j^2 \alpha_x(i\xi_j)\,\mathrm{Tr}\,[\mathbf{G}(\mathbf{r},\mathbf{r},i\xi)], \qquad (6)$$

where $x=\{r,g\}$ and $\xi_j = 2\pi j k_B T/\hbar$ are the Matsubara frequencies (the primed summation indicates a factor of $1/2$ for $j=0$). The nonresonant energy shift reduces to the zero-temperature results if the condition $k_B T \ll (\hbar c/z_+)$ holds. Here, z_+ is the maximum atom-surface distance, which is given by $z_+ = d + \Delta z$, where Δz is the temperature-induced displacement. For the setup proposed in the main text, $T=30$ mK, $d=0.7$ μm and $\Delta z = 2.8$ pm, the ratio becomes $k_B T/(\hbar c/z_+) \simeq O(10^{-6}) \ll 1$. This ensures that the above expression for nonresonant energy-shift contribution reduces

to its zero temperature counterpart, as used in Eqs. (1) and (2). The finite-temperature resonant contribution is given by

$$\delta\omega_r^{R} = \frac{\mu_0}{3}\sum_{k>r} n_{\mathrm{p}}(\omega_{rk})\omega_{kr}^2|\mathbf{d}_{kr}|^2\mathrm{Tr}[\mathrm{Re}[\mathbf{G}(\mathbf{r},\mathbf{r},\omega_{kr})]]$$
$$-\frac{\mu_0}{3}\sum_{k<r}[n_{\mathrm{p}}(\omega_{rk})+1]\omega_{rk}^2|\mathbf{d}_{rk}|^2\mathrm{Tr}[\mathrm{Re}[\mathbf{G}(\mathbf{r},\mathbf{r},\omega_{rk})]],$$

(7)

with $n_{\mathrm{p}}(\omega_{rk}) = [e^{\hbar\omega_{rk}/k_BT} - 1]^{-1}$ denoting the EM field occupation number. The first term accounts for the decay of an atomic state to its lower states ($k < r$); the second term represents the thermally activated excitations. In both terms, the thermal-induced transitions are nonzero only if $n_{\mathrm{p}}(\min[\omega_{rk}]) > 1$, i.e., if the lowest frequency $\min[\omega_{rk}]$ within the transition manifold is thermally actuated. For the Rydberg manifold $|80S_{1/2}\rangle$, $\min[\omega_{rk}] = 2\pi \times 46.93$ GHz (i.e., transition from $|r = 80S_{1/2}\rangle \to |k = 79P_{3/2}\rangle$), and temperature $T = 30$ mK, we get $n_{\mathrm{p}}(\min[\omega_{rk}]) = O(10^{-32})$. This validates the zero-temperature limit in Eq. (3). A similar analysis can be performed for the decay rate, thus providing justification for Eq. (5). This stems from the fact that thermal correction appears through a factor $n_{\mathrm{p}}(\omega_{rk})$ [26], which we show to be negligible.

In particular, we take the values $E_{\mathrm{F}} \simeq 0.8$ eV and $\gamma_g = 10^{12}$ s^{-1} for the graphene Fermi energy and relaxation rate, respectively [28–31].

III. SIDEBAND COOLING OF THE GRAPHENE FLEXURAL MODE

Let us begin by describing the coupling mechanism between the out-of-plane (flexural) vibration of the graphene resonator and the Rydberg atomic state. For a fixed atom-surface distance d, the atomic transition frequency is given by

$$\omega_a = \omega_0 + \delta\omega(d),$$

(8)

where ω_0 is the free space transition frequency and $\delta\omega(d) \equiv \delta\omega_r(d) - \delta\omega_g(d)$ is surface-induced shift. CP energy shift are extremely sensitive to small distance variations. In the nonretarded limit, i.e., the atom-surface distance is less than the effective transition wavelength, this shift scales as $\approx(d + \delta z)^{-3}$ where δz are small deviations from the equilibrium. Thus, as the suspended graphene vibrates out of plane, this motion will induce a modulation in the local Rydberg transition frequency, where $\delta\omega(d) \to \delta\omega(d + \delta z)$.

For small amplitudes, $\delta z \ll d$, one can write the total Hamiltonian of the system as [9,32]

$$\hat{H} = \hbar\omega_m \hat{b}^\dagger \hat{b} + \hbar\frac{\Omega}{2}\sigma_x - \hbar\frac{\Delta}{2}\sigma_z + \hbar g(\hat{b} + \hat{b}^\dagger)\sigma_z.$$

(9)

The first term is the graphene mechanical oscillator Hamiltonian, with $\hat{b}$ ($\hat{b}^\dagger$) standing for the phonon annihilation (creation) operator; the second term describes the Rydberg laser driving of effective Rabi frequency Ω and detuning Δ with respect to local Rydberg transition frequency [9,32,33]. Finally, the last term in Eq. (9) is the (electromechanical) interaction between the atom and the oscillating surface with
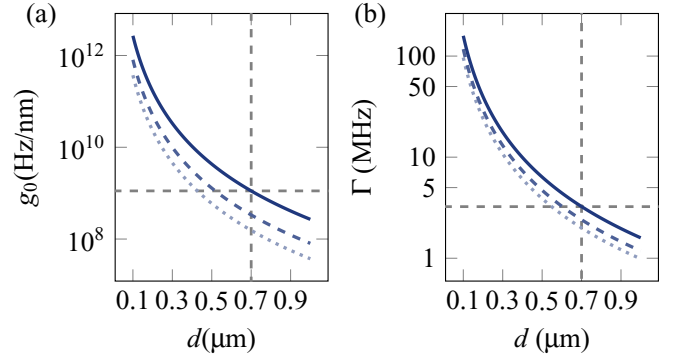

FIG. 2. (a) Casimir-Polder vacuum coupling g_0 and (b) spontaneous decay rate Γ of the Rydberg states $|80S_{1/2}\rangle$ (solid line), $|60S_{1/2}\rangle$ (dashed line), and $|50S_{1/2}\rangle$ (dotted line). The intersection of gray lines fixes our chosen working point at $d = 0.7$ μm.

effective coupling $g = g_0 z_{\mathrm{zpf}}$, with

$$g_0 = \partial_z\delta\omega(d)|_{z=d}.$$

(10)

Here, g_0 is the CP coupling describing the amount of the change in the atomic transition frequency per unit displacement in graphene motion. The quantity $z_{\mathrm{zpf}} = \sqrt{\hbar/2m\omega_m}$ is the zero-point fluctuation of the oscillator, characterized by its effective mass m and frequency ω_m, and the position operator is given by $\hat{z} = z_{\mathrm{zpf}}(\hat{b} + \hat{b}^\dagger)$. In Fig. 2, we depict the vacuum coupling g_0 and the effective Rydberg decay rate Γ as a function of the atom-surface distance different Rydberg states at zero temperature,[1] observing their enhancement due to the Rydberg physics [34]. While the free-space spontaneous decay rate of a Rydberg state is of the order of a few kHz, the presence of a macroscopic surface increases these values only up to few MHz for the micron-scale distances considered here.

Hamiltonians similar to Eq. (9) are used for reservoir-engineering schemes, which are at the basis of different ground-state cooling solutions, achieved for single ions [35], optomechanical setups [36–38], single atoms [39], and nitrogen-vacancy centers in diamond [40]. These have also been recently proposed for carbon nanotubes [41–43]. The cooling scheme proposed in this article is based on a similar protocol, where graphene phonons are scattered away through the sufficiently fast relaxation of the Rydberg atomic degrees of freedom (DOF), to which the graphene flexural mode is coupled via the CP forces. To achieve resolved sideband cooling in this process, the following criteria are to be fulfilled [40,44,45]:

    (i) weak effective coupling, $g/\Gamma < 1$;

    (ii) atomic resolved sidebands, $\Gamma/\omega_m < 1$;

    (iii) strong cooperativity, $g^2/\Gamma(\gamma_m n_{\mathrm{th}}) > 1$.

Here, γ_m is the mechanical damping rate and n_{th} is the initial mean thermal phonon in the mechanical mode. From these conditions, it turns out that the strong cooperativity is improved by the enhancement of the vacuum coupling g_0, as

---

[1] The transition frequencies and the matrix elements of the dipole operator for the Rydberg states can be calculated by using the Numerov method and by employing the Clebsch-Gordan coefficients.

$g = g_0 z_{\rm zpf}$. At the same time, to fulfill the weak-coupling condition, a smaller value of g is required. Moreover, both the resolved sideband and the strong cooperativity conditions are reinforced by the smaller values of the effective atomic decay rate Γ. To fulfill all these conditions simultaneously, the cooling protocol requires a delicate balance among the competing parameters.

In the low-temperature regime and nonretarded limit, the CP potential and transitions rates for a Rydberg atom scale as $\propto n^4/z^3$ [34], leading to decay rates on the order of a few MHz for the atom-surface distances of a few microns (see Fig. 2). On the other hand, low-excited states, which have a free-space decay rate on the order of MHz, can be surface-enhanced to a value which might violate the above conditions. Therefore, a low-lying state would not be suitable for sideband cooling. In the proposed scheme, the freedom to vary the atom-surface distance as well as the principal quantum number of the Rydberg state allows us to be in the regime where sideband cooling would be feasible for graphene flexural modes. However, there are some constraints when working with Rydberg atoms that need to be addressed. Although we have the freedom to tune n and z, we have to take into account that the atomic size of the atom scales with n^2. Due to its increasing size, there is a limit to how close it can be from the surface [25]. Having these constraints in mind, operating at $d = 0.7$ μm and $n = 80$ (see dashed line in Fig. 2), we find $g_0 = 1.12$ GHz/nm (correspondingly, $g = 0.57$ MHz) and $\Gamma = 3.24$ MHz, with the conditions (i) $g/\Gamma \simeq 0.18 < 1$ and (ii) $\Gamma/\omega_m \simeq 0.03 < 1$ being simultaneously satisfied. Only condition (iii) remains to be met. To do so, we consider a flexuron initially in equilibrium with a bath at temperature $T = 30$ mK. Furthermore, we consider a graphene resonator of mass $m = 1.6 \times 10^{-18}$ kg and quality factor $Q = 2 \times 10^5$ (see, e.g., Refs. [6,46]). The graphene resonator frequency is then $\omega_m = 2\pi \times 20$ MHz for which we find $\bar{n}_{\rm th} \simeq 30$. Combining these results, we can finally satisfy condition (iii) $g^2/\Gamma(\gamma_m n_{\rm th}) \simeq 5.2 > 1$.

IV. ANALYSIS OF THE COOLING PROCESS

Taking advantage of the features of Rydberg atoms discussed above, we now construct a resolved sideband cooling scheme for the fundamental flexural mode of a graphene resonator. We first present a unitary picture of the cooling process by considering the Hamiltonian appearing in Eq. (9) and by transforming it into the basis in which the effective two-level atom is diagonal, which reads

$$\hat{H} = -\hbar \frac{\omega_s}{2}\sigma_z + \hbar \omega_m \hat{b}^\dagger \hat{b}$$
$$+ \hbar[g\cos(\alpha)\sigma_z - g\sin(\alpha)\sigma_x](\hat{b} + \hat{b}^\dagger), \quad (11)$$

where $\omega_s = (\Delta^2 + \Omega^2)^{1/2}$ is the energy splitting of two dressed states:

$$|+\rangle = \sin(\alpha/2)|g\rangle + \cos(\alpha/2)|r\rangle,$$
$$|-\rangle = \cos(\alpha/2)|g\rangle - \sin(\alpha/2)|r\rangle,$$

with $\tan\alpha = \Omega/|\Delta|$, $\sin(\alpha) = \Omega/\omega_s$, and $\cos(\alpha) = -\Delta/\omega_s$. Then we move to the interaction picture via the unitary transformation $\hat{U} = \exp[i(\omega_m \hat{b}^\dagger \hat{b} + (\omega_s/2)\sigma_z)t]$. After performing

a rotating wave approximation (RWA) (valid for $g \ll \omega_s = \omega_m$), we recast Eq. (11) as

$$\hat{H}_I = \hat{U}^\dagger \hat{H}\hat{U} = -\hbar \tilde{g}(\sigma_- \hat{b}^\dagger + \sigma_+ \hat{b}), \quad (12)$$

with $\tilde{g} = g\sin(\alpha)$.

In the single-phonon picture, the Hamiltonian (12) drives the transition $|-, n\rangle \leftrightarrow |+, n-1\rangle$, where $|n\rangle$ is the phonon Fock basis. Since the atomic decays are fast, $\Gamma > \tilde{g}$, and the latter is overdamped, which guarantees that phonons can be damped away thanks to the dressing with the atomic degrees of freedom. Note that, in the dressed-states picture, the resonance condition occurs when the laser induced atomic energy splitting is equal to the mechanical frequency, as given by $\omega_s = \omega_m$.

The dynamics of the open system is governed by the Markov master equation

$$\dot{\rho} = -(i/\hbar)[\hat{H}, \hat{\rho}] + \mathcal{L}(\hat{\rho}), \quad (13)$$

where the Liouville operator, accounting for irreversible dynamics due to the coupling with the various dissipative channels, is given by

$$\mathcal{L}(\hat{\rho}) = \frac{\gamma_m}{2}(\bar{n}_{\rm th} + 1)\mathcal{D}_{\hat{b}}[\hat{\rho}] + \frac{\gamma_m}{2}\bar{n}_{\rm th}\mathcal{D}_{\hat{b}^\dagger}[\hat{\rho}]$$
$$+ \Gamma \mathcal{D}_{\hat{\sigma}_-}[\hat{\rho}] + \frac{\tilde{\Gamma}}{4}\mathcal{D}_{\hat{\sigma}_z}[\hat{\rho}], \quad (14)$$

with $\mathcal{D}_{\hat{o}}[\hat{\rho}] = 2\hat{o}\hat{\rho}\hat{o}^\dagger - \hat{o}^\dagger \hat{o}\hat{\rho} - \hat{\rho}\hat{o}\hat{o}^\dagger$. The first and second terms in Eq. (14) describe the thermalization process with the phonon bath, respectively accounting for the (stimulated and spontaneous) thermal emission and thermal excitation of the mechanical mode of vacuum decay rate $\gamma_m = \omega_m/Q$. The third term describes the atomic spontaneous emission in the presence of a graphene resonator Γ; the fourth term accounts for the atomic dephasing occurring at the rate $\tilde{\Gamma}$. Note that, for the cryogenic temperatures considered, we can safely neglect the atomic thermal excitation.

In the Lamb-Dicke regime, $g\sqrt{\bar{n}_{\rm th} + 1} < \omega_m$ [47], where the mode-atom interaction is only a perturbative effect, the system will relax into the product state $\hat{\rho}(t) \simeq \hat{\rho}_{\rm ss} \otimes \hat{\rho}_m(t)$, which will be composed of the atomic steady-state density matrix $\hat{\rho}_{ss}$ and the reduced mechanical density matrix $\hat{\rho}_m = \text{Tr}_a[\rho]$, with the trace performed over the atomic degrees. This allows us to adiabatically eliminate the atomic degrees and rewrite the master equation for the mechanical modes alone [44],

$$\dot{\hat{\rho}}_m = -i\omega_m[\hat{b}^\dagger \hat{b}, \hat{\rho}_m] + A_-\mathcal{D}_{\hat{b}}[\hat{\rho}_m] + A_+\mathcal{D}_{\hat{b}^\dagger}[\hat{\rho}_m], \quad (15)$$

where

$$A_- = g^2 S(\omega_m) + (\gamma_m/2)(\bar{n}_{\rm th} + 1), \quad (16)$$

$$A_+ = g^2 S(-\omega_m) + (\gamma_m/2)\bar{n}_{\rm th} \quad (17)$$

describe the effective flexural cooling and heating rates, respectively. These processes are a result of the coupling to the dissipative atomic bath, characterized by its steady-state spectral density [48]

$$S(\omega) = \text{Re}\left[\int_0^\infty d\tau e^{i\omega\tau} \langle \delta\sigma_z(\tau)\delta\sigma_z\rangle_{\rm ss}\right]. \quad (18)$$
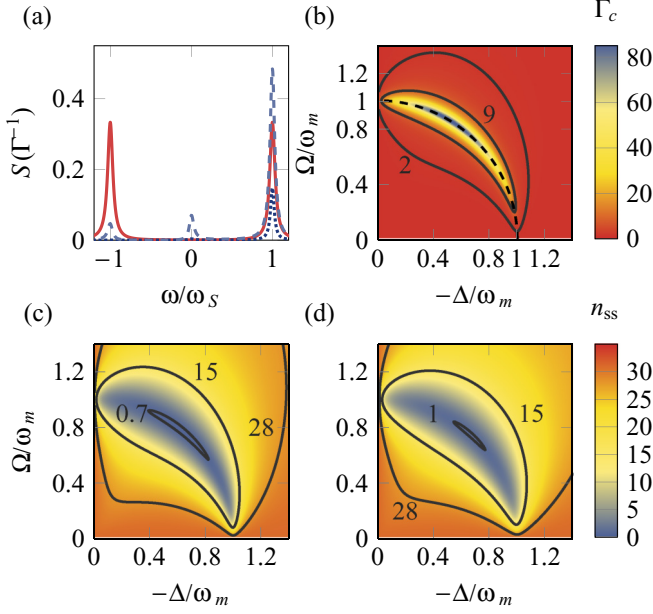
FIG. 3. (a) Real part of the atomic spectrum for $\Omega = 0.85\,\omega_m$ (dashed line), $\Omega = \omega_m$ (solid line) and $\Omega = 0.4\,\omega_m$ (dotted line), with peaks $\omega_s = \pm(\Omega^2 + \Delta^2)^{1/2}$. Optimal driving is achieved for $\Omega = 0.85\,\omega_m$. For $\Omega = \omega_m$, the heating and cooling peak balance each other, therefore, the coupled atomic system does not work as a cold bath. (b) Net cooling rate Γ_c (in units of kHz) of the graphene resonator. (c) Steady-state phonon number n_{ss}. (d) The same as in panel (c) but considering a dephasing rate $\tilde{\Gamma} = 0.015\,\omega_m$. For panels (b)–(d), we have set $\omega_m = 2\pi \times 20$ MHz and $m = 1.6 \times 10^{-18}$ kg.

The spectrum is determined by the correlation of the atomic steady-state fluctuation operator $\delta\sigma_z = \sigma_z - \langle\sigma_z\rangle_{ss}$ and obtained by solving Bloch's equations for the Rydberg atom alone [cf. Eq. (14)] and by applying the quantum regression theorem [48] (see more information in Appendix B). Note that the cooling and heating rates are evaluated at positive ω_m and negative $-\omega_m$ frequencies. This characterizes the ability of the atom to respectively absorb and emit phonons at that very frequency [49]. As one can see from Eq. (15), one must enhance the phonon absorption in detriment of its emission, in order to increase the effective flexural cooling rate. This means that we need to look at optimal parameters that enhance the positive frequency component of the (asymmetric) spectrum.

In Fig. 3(a), we have plotted the steady-state spectrum for different Rabi frequencies. As we can see, $S(\omega)$ exhibits three well-resolved peaks at $\omega = 0$ and $\omega = \pm\omega_s$. In the resolved sideband regime, $\Gamma \ll \omega_s$, the optimal cooling conditions (i.e., when the phonon absorption capacity by the atom is maximized) are achieved at resonance $\omega_s = \omega_m$ for a driving strength of $\Omega \simeq 0.85\,\omega_m$ [44,50] (see more details in Appendix B). In the interaction picture, the process $|-, n\rangle \mapsto |+, n-1\rangle$ corresponds to cooling, which is manifested by the peak at $\omega = \omega_s$. Such cooling is obtained for red detuned driving, $\omega_l - \omega_a = -\Delta$. From Eq. (15), one can recast the rate equation for the mean flexural number,

$$\langle \dot{n}\rangle \equiv \mathrm{Tr}[\dot{\hat{\rho}}_m \hat{b}^\dagger \hat{b}] = -\Gamma_c\langle n\rangle + A_+, \qquad (19)$$
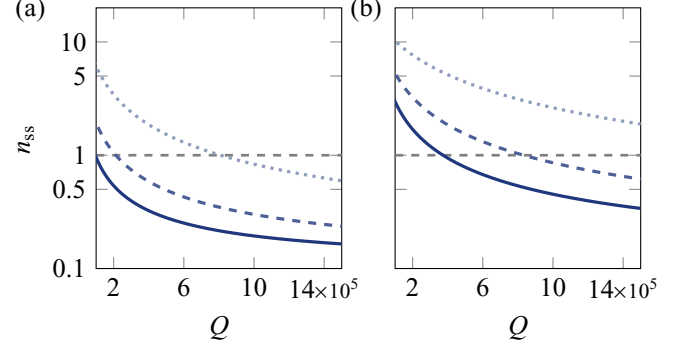

FIG. 4. (a) Final occupation number n_{ss} for optimal cooling conditions (see text) as a function of mechanical quality factor Q. Rydberg state $|80S_{1/2}\rangle$ with $T = 30$ mK. (b) Rydberg state $|60S_{1/2}\rangle$ with $T = 15$ mK. In both panels, distances correspond to $d = 0.7\ \mu$m (solid line), $d = 0.8\ \mu$m (dashed line), and $d = 1.0\ \mu$m (dotted line). The horizontal dashed line sets the ground-state cooling threshold.

where the net cooling rate is given by $\Gamma_c = A_- - A_+$. Ground-state cooling is achieved if the steady-state flexuron number, $n_{ss} = A_+/\Gamma_c$, satisfies the condition $n_{ss} < 1$. Using Eq. (15) leads us the optical cooling rate γ_{opt} and the minimal occupation number n_0 (see Appendix C for further details), reading

$$\gamma_{opt} = 2g^2[S(\omega_m) - S(-\omega_m)], \qquad (20)$$

$$n_0 = \frac{S(-\omega_m)}{S(\omega_m) - S(-\omega_m)}. \qquad (21)$$

The net cooling rate Γ_c and the steady-state phonon number n_{ss} take the form

$$\Gamma_c = \frac{1}{2}(\gamma_{opt} + \gamma_m), \quad n_{ss} = \frac{\gamma_{opt}n_0 + \gamma_m \bar{n}_{th}}{\gamma_{opt} + \gamma_m}. \qquad (22)$$

Since $\gamma_{opt} \sim (g^2/\Gamma) \gg \gamma_m$, one can then write $n_{ss} \simeq n_0 + (\gamma_m \bar{n}_{th}/\gamma_{opt})$. Given that the heating process [related to the peak $S(-\omega_m)$] is highly suppressed, the final occupation number is limited by the smallness of the ratio $\gamma_m \bar{n}_{th}/\gamma_{opt}$, which is guaranteed for large values of g and the small values of Γ. The high polarizability of the Rydberg state provides such a requirement.

In Fig. 3(b), we plot the cooling rate Γ_c. The maximum of the cooling rate occurs at resonance $\omega_s = \omega_m$ with the (optimal) driving $\Omega \simeq 0.85\omega_m$, for which the asymmetry in the atomic spectra is the largest, thus manifesting the utmost phonon absorption capacity by the atom. Moreover, the steady-state phonon number is shown in Fig. 3(c). For the optimal cooling conditions, we get a record value $n_{ss} \lesssim 0.7$ for an atom-surface distance $d = 0.7\ \mu$m. However, ground-state cooling of the flexural modes might be obtained also for larger atom-surface distances by tuning the mechanical quality factor of the graphene sheet. In Fig. 4(a), we plot the ground-state occupancy against the quality factor for the range of values achievable in state-of-the-art experiments [51]. Furthermore, in Fig. 4(b), we show that, if we set the initial temperature $T = 15$ mK, a Rydberg state $|60S_{1/2}\rangle$ can also lead to ground-state cooling at $d = 0.8\ \mu$m with $Q = 10^6$.

Finally, we investigate how robust the ground-state cooling protocol can be in the presence of dephasing, which may
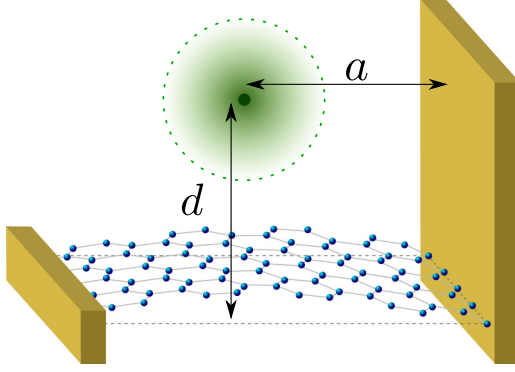
FIG. 5. Schematic representation of a possible experimental setup, not to scale. A vertical atom-chip surface is used to magnetically trap a Rydberg atom next to a suspended graphene membrane. The horizontal distance a is much larger than the vertical atom-graphene distance.

enter the cooling dynamics as a result of the atomic trap fluctuations and surface-induced noise. In fact, provided that the condition $\tilde{\Gamma} < \omega_m$ is satisfied, ground-state cooling is still attained. This fact is patent in Fig. 3(d), revealing that $n_{ss} \lesssim 1$ for $\tilde{\Gamma} = 0.015\,\omega_m$, which is estimated to be met in typical conditions [52,53]. These dephasing effects will set a cooling threshold, clearly shortening the region of parameters for which ground-state cooling is achievable. It is therefore desirable to understand at which extent dephasing effects can be mitigated or controlled in state-of-the-art experimental conditions, although our calculations seem to suggest that our protocol is quite robust.

V. EXPERIMENTAL FEASIBILITY

Trapping and control of single Rydberg atoms has quite recently become a reality [54]. It has been experimentally possible to trap [55,56] and excite to Rydberg states at large [57] and submicron distances [58] from the surfaces. By combining these methods with our proposal, it would be possible to experimentally realize the cooling protocol described here. In Ref. [57], ^{87}Rb Rydberg atoms have been trapped in a chip-surface magnetic field. This scheme is obtained at a chip-atom distance of 100 μm. At such distances, CP effects are very small, even for Rydberg atoms. In our setup, we propose to magnetically trap atoms in a staircase configuration, as shown in Fig. 5. The chip surface would then be placed perpendicular to the graphene sheet. This would then allow us to trap magnetically the atom at horizontal distances a of the order of hundred micrometres, but at the same time to have vertical atom-graphene distances d of the order of hundreds of nanometers. Another possibility would be to prepare a hosting surface of ^{87}Rb using the same techniques as presented in Ref. [31] for Er^{3+}. Furthermore, while we have demonstrated the cooling effects through fully available transition data of ^{87}Rb, solid-state semiconductor Rydberg excitons in bulk Cu_2O [59] could also be used to implement our cooling scheme.

VI. CONCLUSIONS

We have constructed a protocol enabling ground-state sideband cooling of out-of-plane (flexural) mode in suspended graphene based on vacuum forces. Our setup consists of a driven Rydberg atom placed a few micrometres away from a graphene nanoresonator, which is coupled with the help of CP forces. Given the high atomic polarizability of Rydberg atoms, the conditions for resolved-sideband cooling are achievable, enabling us to bring the fundamental flexural mode down to the quantum limit. Our findings overcome the difficulty associated with cooling schemes based on optomechanical laser cooling (a fact inherited from the large light absorbency of graphene in usual optomechanical interfaces), thus paving the way towards practical applications in quantum technology for which quantum motion is necessary. Moreover, this may also contribute to the enrichment of condensed-matter platforms, because flexural modes are known to strongly affect the electronic mobility in suspended graphene [60]. For example, we anticipate that our scheme could be used to control the emission of graphene plasmons [31], eventually potentiating the generation of plasmon lasers and control of the emission properties of atomic Rydberg states [61,62].

APPENDIX A: SURFACE-SCATTERED GREEN'S FUNCTION AND GRAPHENE PROPERTIES

The scattered EM field is characterized by the dyadic Green's function **G**, which is the solution of the Helmholtz equation

$$[(\nabla \times \nabla \times) - (\omega^2/c^2)\epsilon(\mathbf{r},\omega)]\mathbf{G}(\mathbf{r},\mathbf{r}',\omega) = \delta(\mathbf{r}-\mathbf{r}') \otimes \mathbb{I}.$$

It encompasses the effects of graphene via its optical conductivity σ and the transverse electric R_{TE} (s polarized) and transverse magnetic R_{TM} (p polarized) reflection coefficients [26],

$$\mathbf{G}(z,z,\omega) = \frac{i}{8\pi} \int_0^\infty dk_\parallel \frac{k_\parallel}{k_\perp} e^{2ik_\perp z}$$

$$\times \mathrm{diag}\left[R_{TE} - \left(\frac{c^2 k_\perp^2}{\omega^2}\right) R_{TM}, R_{TE} \right.$$

$$\left. - \left(\frac{c^2 k_\perp^2}{\omega^2}\right) R_{TM}, \left(\frac{2c^2 k_\parallel^2}{\omega^2}\right) R_{TM} \right]. \quad (A1)$$

Here, $\mathrm{diag}[\cdot,\cdot,\cdot]$ is a 3×3 diagonal matrix. The free-space wave vector satisfies $k^2 = k_\parallel^2 + k_\perp^2 = (\omega^2/c^2)$, while $k'_\perp = (\epsilon k^2 - k_\parallel^2)^{1/2}$ denotes the wave vector in the graphene plane (for suspended graphene, the medium is vacuum, so $\epsilon = 1$).
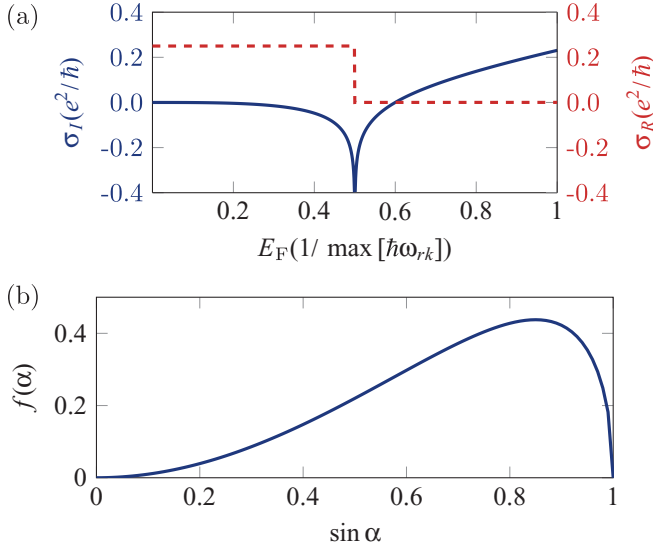
(a)

(b)

FIG. 6. (a) Photonic conductivity behavior of graphene. (b) Dimensionless function $f(\alpha)$.

The Fresnel reflection coefficients $R_{\mathrm{TE}} = R_{\mathrm{TE}}(\omega, k_\parallel)$, $R_{\mathrm{TM}} = R_{\mathrm{TM}}(\omega, k_\parallel)$ are explicitly given by [30]

$$R_{\mathrm{TE}} = -\frac{\mu_0 \sigma \omega}{2k_\perp + \mu_0 \sigma \omega}, \qquad (A2)$$

$$R_{\mathrm{TM}} = \frac{k_\perp \sigma}{k_\perp \sigma + 2\epsilon_0 \omega}. \qquad (A3)$$

To calculate the nonresonant part of the energy shift, we introduce the imaginary frequency $\omega = i\xi$, allowing for a better evaluation of the poles [26]. For the real-frequency dependence, the two regions $0 < k_\parallel < \omega/c$ (propagating waves) and $k_\parallel > \omega/c$ (evanescent waves) are considered in the numerical computation of Eq. (A1). Moreover, the graphene conductivity $\sigma = \sigma(\omega)$ is given within the random phase approximation (RPA), whose real $\sigma_R(\omega)$ and imaginary $\sigma_I(\omega)$ parts take the form [30]

$$\sigma_R(\omega) = \frac{e^2 E_{\mathrm{F}}}{\pi \hbar^2} \frac{1/\tau}{\omega^2 + 1/\tau^2} + \frac{e^2}{4\hbar} \theta(\hbar\omega - 2E_{\mathrm{F}}), \quad (A4)$$

$$\sigma_I(\omega) = \frac{e^2 E_{\mathrm{F}}}{\pi \hbar^2} \frac{\omega}{\omega^2 + 1/\tau^2} - \frac{e^2}{4\pi\hbar} \ln \left| \frac{2E_{\mathrm{F}} + \hbar\omega}{2E_{\mathrm{F}} - \hbar\omega} \right|, \quad (A5)$$

where $\tau = 1/\gamma_g$ denotes the electron-scattering time. The typical behavior of both the real and imaginary parts of the optical conductivity is shown in Fig. 6(a). For $E_{\mathrm{F}} \lesssim 0.5 \max[\hbar\omega_{rk}]$, the conductivity is mostly real and the atomic transition decay dumps energy into the particle-hole (interband) continuum. In the region $0.5 \max[\hbar\omega_{rk}] \lesssim E_{\mathrm{F}} \lesssim 0.7 \max[\hbar\omega_{rk}]$, the atom decays into free space, while for $E_{\mathrm{F}} \gtrsim 0.7 \max[\hbar\omega_{rk}]$ the decay process results in a plasmon excitation (intraband), as witnessed by a positive imaginary part in the conductivity [31].

It is well known (and hereby also verified by our numerical calculations) that the shift in the state $|\bar{n}S_{1/2}\rangle$ is mainly due to the neighboring transition $|\bar{n}S_{1/2}\rangle \rightarrow |k = (\bar{n}-1)P_{1/2,3/2}\rangle$ ($\bar{n}$ being the principal quantum number), i.e., the transition of lowest frequency (i.e., $\min[\hbar\omega_{rk}] \simeq 0.0308$ meV) and largest dipole moment [34]. For $\bar{n} = 80$, the choice of the Fermi en-

ergy in the main text ($E_{\mathrm{F}} = 0.8$ eV) suggests that emissions in this frequency range result in plasmon excitations for almost $\simeq 97\%$ of the whole transition manifold, as the condition $E_{\mathrm{F}} \gtrsim 0.7[\hbar\omega_{rk}]$ is fulfilled. Therefore, only a small percentage of the transitions (and thus with a negligible contribution to the atomic energy shifts) will emit in the particle-hole continuum. Both intra- and interband emissions could potentially heat graphene via the sequential excitation of in-plane phonons. However, their effect in the heating via the production of out-of-plane phonons (flexurons) are unknown. Although interesting, the latter are out of the scope of the present work.

APPENDIX B: ATOMIC DRESSED STATES AND THEIR POWER SPECTRUM

Coming back to Eq. (14) of the main text, we can obtain the dynamics of the Bloch vector $\vec{\sigma} = [\sigma_x, \sigma_y, \sigma_z]^T$ from the isolated Bloch equation, i.e., considering only the atomic part of the Hamiltonian, thus taking $\gamma_m = 0$. In the limit of pure atomic decay (i.e., $\tilde{\Gamma} \rightarrow 0$), the Bloch vector evolves as

$$\partial_t \langle \vec{\sigma} \rangle = A \langle \vec{\sigma} \rangle - \vec{\Gamma}, \qquad (B1)$$

where

$$A = \begin{pmatrix} -\Gamma & -\omega_s \cos(\alpha) & 0 \\ \omega_s \cos(\alpha) & -\Gamma & -\omega_s \sin(\alpha) \\ 0 & \omega_s \sin(\alpha) & 2\Gamma \end{pmatrix}, \quad (B2)$$

$$\vec{\Gamma} = \begin{pmatrix} 0 \\ 0 \\ 2\Gamma \end{pmatrix}. \qquad (B3)$$

Using the quantum regression theorem [44], one can write the spectrum $\mathcal{S}(\omega) = \langle \delta\sigma_z(-i\omega)\delta\sigma_z(0)\rangle_{\mathrm{ss}}$ for the steady-state correlation of the fluctuation operator $\delta\sigma_z$ (defined in the main text) as

$$\mathcal{S}(\omega) = -(0, 0, 1) \cdot [i\omega \mathbf{1} + A]^{-1}\vec{B}, \qquad (B4)$$

where $\vec{B} = \langle \delta\vec{\sigma} \delta\sigma_z \rangle_{\mathrm{ss}}$. Given the inverse of the matrix $[i\omega \mathbf{1} + A]^{-1} = \mathrm{adj}[i\omega \mathbf{1} + A]/\det[i\omega \mathbf{1} + A]$ (with adj[.] and det[.] denoting the adjugate and determinant, respectively), one can write

$$\mathcal{S}(\omega) = \frac{h(\omega)}{(i\omega + \epsilon_0)(i\omega + \epsilon_+)(i\omega + \epsilon_-)}, \qquad (B5)$$

where $h(\omega) = -(0, 0, 1) \cdot \mathrm{adj}[i\omega \mathbf{1} + A]^{-1}\vec{B}$. Here, ϵ_i are the eigenvalues of matrix A. The spectrum generally exhibits three peaks, whose frequencies and width are respectively given by the imaginary and real parts of ϵ_i. In the resolved sideband regime, $\Gamma/\omega_s \ll 1$, the eigenvalues are given by

$$\epsilon_0 \simeq -\Gamma_{\epsilon_0}, \quad \epsilon_\pm \simeq \pm i\omega_s - \Gamma_{\epsilon_+},$$

where

$$\Gamma_{\epsilon_0} = \frac{\Gamma}{2}[\cos(2\alpha) + 3], \quad \Gamma_{\epsilon_+} = \frac{\Gamma}{4}[\cos(2\alpha) - 5].$$

It is therefore clear that the spectrum exhibits well-resolved peaks at $\omega = (0, \pm\omega_s)$, as illustrated in Fig. 3(a) of the paper. In the same regime, the real part of the spectrum in the vicinity of $\pm\omega_s$ reads

$$S(\omega) \equiv \mathrm{Re}[\mathcal{S}(\omega \simeq \pm\omega_s)] = \frac{\Gamma_{\epsilon_+}}{\Gamma_{\epsilon_+}^2 + (\omega \mp \omega_s)} (P_\pm), \quad (B6)$$

with

$$P_{\pm} = \text{Re}\left[\frac{-h(\pm\omega_s)}{(\pm i\omega_s - \Gamma_{\epsilon_0})(\pm 2i\omega_s - \Gamma_{\epsilon_+})}\right] \qquad \text{(B7)}$$

To the lowest order in Γ/ω_s, $P_{\pm}$ is explicitly given by

$$P_+ = \frac{\sin^6(\alpha)\csc^4\left(\frac{\alpha}{2}\right)}{4(\cos(2\alpha) + 3)},$$

$$P_- = \frac{4\sin^4\left(\frac{\alpha}{2}\right)\sin^2(\alpha)}{\cos(2\alpha) + 3}.$$

For convenience, we finally define a dimensionless function $f(\alpha) = \Gamma[S(\omega) - S(-\omega)]$, capturing the dependence of the net cooling rate on the relevant parameters of the problem. In the limit $\omega \to \omega_s$, the function turns out to be

$$f(\alpha) = -\frac{8\sin(\alpha)\sin(2\alpha)}{[\cos(2\alpha) - 5][\cos(2\alpha) + 3]}. \qquad \text{(B8)}$$

As can be seen in Fig. 6, this function is peaked at $\Omega \simeq 0.85\omega_s$, revealing the optimal configuration for resolved sideband cooling to take place.

APPENDIX C: CONTRIBUTION BY COUPLED DISSIPATIVE ATOMIC BATH AND NET COOLING RATE

From Eq. (15) of the main text, one can isolate the effects of the thermal bath (the uncontrolled reservoir) and that of the "dissipative atomic bath" (controlled reservoir). This allows us to write the equation in the form

$$\dot{\rho}_m = -i\omega_m[\hat{b}^\dagger\hat{b}, \hat{\rho}_m] + \frac{\gamma_{\text{opt}}}{2}(n_0 + 1)\mathcal{D}_{\hat{b}}[\hat{\rho}_m]$$
$$+ \frac{\gamma_{\text{opt}}}{2}n_0\mathcal{D}_{\hat{b}^\dagger}[\hat{\rho}_m] + \frac{\gamma_m}{2}(\bar{n}_{\text{th}} + 1)\mathcal{D}_{\hat{b}}[\hat{\rho}]$$
$$+ \frac{\gamma_m}{2}\bar{n}_{\text{th}}\mathcal{D}_{\hat{b}^\dagger}[\hat{\rho}], \qquad \text{(C1)}$$

where $\gamma_{\text{opt}} = 2g^2[S(\omega_m) - S(-\omega_m)]$ is the optical cooling rate and $n_0 = S(-\omega_m)/[S(\omega_m) - S(-\omega_m)]$ is the minimal (or residual) flexural occupation number. Both quantities are a result of the coupling to the dissipative atomic bath alone. Conversely, the net cooling rate Γ_c and the steady-state phonon number n_{ss} described in the paper take the form

$$\Gamma_c = \frac{1}{2}(\gamma_{\text{opt}} + \gamma_m), \quad n_{\text{ss}} = \frac{\gamma_{\text{opt}}n_0 + \gamma_m\bar{n}_{\text{th}}}{\gamma_{\text{opt}} + \gamma_m}. \qquad \text{(C2)}$$

Using Eq. (B8) and taking $\omega_s = \omega_m$, the total optical cooling rate reads

$$\gamma_{\text{opt}} \simeq (2g^2/\Gamma)f(\alpha) = \frac{8\sin^2(\alpha)\sqrt{1 - \sin^2(\alpha)}}{4 - \sin^4(\alpha)}\frac{g^2}{\Gamma}. \qquad \text{(C3)}$$

The optical cooling rate turns out to be $O(g^2/\Gamma)$. To achieve ground-state cooling, γ_{opt} must exceed the intrinsic flexural thermal heating rate $\gamma_m\bar{n}_{\text{th}}$. As a consequence, a large value of the ratio $(\gamma_{\text{opt}}/\gamma_m\bar{n}_{\text{th}}) = g^2/\Gamma\gamma_m\bar{n}_{\text{th}}$ (dubbed the cooperativity parameter in the literature) is required to achieve ground-state cooling [50].

[1] J. S. Bunch, A. M. van der Zande, S. S. Verbridge, I. W. Frank, D. M. Tanenbaum, J. M. Parpia, H. G. Craighead, and P. L. McEuen, Science **315**, 490 (2007).

[2] G. A. Steele, A. K. Huttel, B. Witkamp, M. Poot, H. B. Meerwaldt, L. P. Kouwenhoven, and H. S. J. van der Zant, Science **325**, 1103 (2009).

[3] C. Chen, S. Rosenblatt, K. I. Bolotin, W. Kalb, P. Kim, I. Kymissis, H. L. Stormer, T. F. Heinz, and J. Hone, Nat. Nanotechnol. **4**, 861 (2009).

[4] M. Will, M. Hamer, M. Müller, A. Noury, P. Weber, A. Bachtold, R. V. Gorbachev, C. Stampfer, and J. Güttinger, Nano Lett. **17**, 5950 (2017).

[5] J. Moser, A. Eichler, J. Güttinger, M. I. Dykman, and A. Bachtold, Nat. Nanotechnol. **9**, 1007 (2014).

[6] A. Castellanos-Gomez, V. Singh, H. S. J. van der Zant, and G. A. Steele, Ann. Phys. (Berlin, Ger.) **527**, 27 (2015).

[7] G. Luo, Z.-Z. Zhang, G.-W. Deng, H.-O. Li, G. Cao, M. Xiao, G.-C. Guo, L. Tian, and G.-P. Guo, Nat. Commun. **9**, 383 (2018).

[8] V. Singh, S. J. Bosman, B. H. Schneider, Y. M. Blanter, A. Castellanos-Gomez, and G. A. Steele, Nat. Nanotechnol. **9**, 820 (2014).

[9] C. A. Muschik, S. Moulieras, A. Bachtold, F. H. L. Koppens, M. Lewenstein, and D. E. Chang, Phys. Rev. Lett. **112**, 223601 (2014).

[10] S. L. de Bonis, C. Urgell, W. Yang, C. Samanta, A. Noury, J. Vergara-Cruz, Q. Dong, Y. Jin, and A. Bachtold, Nano Lett. **18**, 5324 (2018).

[11] K. E. Khosla, M. R. Vanner, N. Ares, and E. A. Laird, Phys. Rev. X **8**, 021052 (2018).

[12] F. Guinea, M. I. Katsnelson, and M. A. H. Vozmediano, Phys. Rev. B **77**, 075422 (2008).

[13] A. Benyamini, A. Hamo, S. V. Kusminskiy, F. von Oppen, and S. Ilani, Nat. Phys. **10**, 151 (2014).

[14] A. H. C. Neto and K. Novoselov, Rep. Prog. Phys. **74**, 082501 (2011).

[15] M. LaHaye, O. Buu, B. Camarota, and K. Schwab, Science **304**, 74 (2004).

[16] R. A. Barton, I. R. Storch, V. P. Adiga, R. Sakakibara, B. R. Cipriany, B. Ilic, S. P. Wang, P. Ong, P. L. McEuen, J. M. Parpia, and H. G. Craighead, Nano Lett. **12**, 4681 (2012).

[17] S. Thongrattanasiri, F. H. L. Koppens, and F. J. García de Abajo, Phys. Rev. Lett. **108**, 047401 (2012).

[18] H. Yan, X. Li, B. Chandra, G. Tulevski, Y. Wu, M. Freitag, W. Zhu, P. Avouris, and F. Xia, Nat. Nanotechnol. **7**, 330 (2012).

[19] X. Song, M. Oksanen, J. Li, P. J. Hakonen, and M. A. Sillanpää, Phys. Rev. Lett. **113**, 027404 (2014).

[20] R. D. Alba, F. Massel, I. R. Storch, T. S. Abhilash, A. Hui, P. L. McEuen, H. G. Craighead, and J. M. Parpia, Nat. Nanotechnol. **11**, 741 (2016).

[21] X. Li, W. Nie, A. Chen, and Y. Lan, Phys. Rev. A **96**, 063819 (2017).

[22] M. Abdi and M. B. Plenio, Phys. Rev. Lett. **122**, 023602 (2019).

[23] J. D. Carter and J. D. D. Martin, Phys. Rev. A **83**, 032902 (2011).

[24] S. D. Hogan, J. A. Agner, F. Merkt, T. Thiele, S. Filipp, and A. Wallraff, Phys. Rev. Lett. **108**, 063004 (2012).

[25] S. Ribeiro and S. Scheel, Phys. Rev. A **88**, 052521 (2013).

[26] S. Buhmann, *Dispersion Forces II: Many-Body Effects, Excited Atoms, Finite Temperature and Quantum Friction* (Springer, 2013), Vol. 248.

[27] S. Scheel and S. Buhmann, Acta Phys. Slovaca **58**, 675 (2008).

[28] C.-F. Chen, C.-H. Park, B. W. Boudouris, J. Horng, B. Geng, C. Girit, A. Zettl, M. F. Crommie, R. A. Segalman, S. G. Louie *et al.*, Nature (London) **471**, 617 (2011).

[29] D. K. Efetov and P. Kim, Phys. Rev. Lett. **105**, 256805 (2010).

[30] F. H. L. Koppens, D. E. Chang, and F. J. García de Abajo, Nano Lett. **11**, 3370 (2011).

[31] K. Tielrooij, L. Orona, A. Ferrier, M. Badioli, G. Navickaite, S. Coop, S. Nanot, B. Kalinic, T. Cesca, L. Gaudreau *et al.*, Nat. Phys. **11**, 281 (2015).

[32] H. Bernien, S. Schwartz, A. Keesling, H. Levine, A. Omran, H. Pichler, S. Choi, A. S. Zibrov, M. Endres, M. Greiner, V. Vuletić, and M. D. Lukin, Nature (London) **551**, 579 (2017).

[33] Y. Zhang, J. Fan, J.-Q. Liang, J. Ma, G. Chen, S. Jia, and F. Nori, Sci. Rep. **5**, 11510 (2015).

[34] J. A. Crosse, S. A. Ellingsen, K. Clements, S. Y. Buhmann, and S. Scheel, Phys. Rev. A **82**, 010901(R) (2010).

[35] F. Diedrich, J. C. Bergquist, W. M. Itano, and D. J. Wineland, Phys. Rev. Lett. **62**, 403 (1989).

[36] F. Marquardt, J. P. Chen, A. A. Clerk, and S. M. Girvin, Phys. Rev. Lett. **99**, 093902 (2007).

[37] A. Schliesser, R. Rivière, G. Anetsberger, O. Arcizet, and T. J. Kippenberg, Nat. Phys. **4**, 415 (2008).

[38] J. D. Teufel, T. Donner, D. Li, J. W. Harlow, M. S. Allman, K. Cicak, A. J. Sirois, J. D. Whittaker, K. W. Lehnert, and R. W. Simmonds, Nature (London) **475**, 359 (2011).

[39] J. D. Thompson, T. G. Tiecke, A. S. Zibrov, V. Vuletić, and M. D. Lukin, Phys. Rev. Lett. **110**, 133001 (2013).

[40] E. MacQuarrie, M. Otten, S. Gray, and G. Fuchs, Nat. Commun. **8**, 14358 (2017).

[41] P. Stadler, W. Belzig, and G. Rastelli, Phys. Rev. Lett. **113**, 047201 (2014).

[42] S. Zippilli, G. Morigi, and A. Bachtold, Phys. Rev. Lett. **102**, 096804 (2009).

[43] X. Wang, A. Miranowicz, H.-R. Li, and F. Nori, Phys. Rev. B **95**, 205415 (2017).

[44] K. Jaehne, K. Hammerer, and M. Wallquist, New J. Phys. **10**, 095019 (2008).

[45] M. Abdi, M.-J. Hwang, M. Aghtar, and M. B. Plenio, Phys. Rev. Lett. **119**, 233602 (2017).

[46] P. Weber, J. Güttinger, A. Noury, J. Vergara-Cruz, and A. Bachtold, Nat. Commun. **7**, 12496 (2016).

[47] I. Wilson-Rae, P. Zoller, and A. Imamoglu, Phys. Rev. Lett. **92**, 075507 (2004).

[48] H.-P. Breuer, F. Petruccione *et al.*, *The Theory of Open Quantum Systems* (Oxford University Press on Demand, Oxford, 2002).

[49] A. A. Clerk, M. H. Devoret, S. M. Girvin, F. Marquardt, and R. J. Schoelkopf, Rev. Mod. Phys. **82**, 1155 (2010).

[50] P. Rabl, Phys. Rev. B **82**, 165320 (2010).

[51] J. Güttinger, A. Noury, P. Weber, A. M. Eriksson, C. Lagoin, J. Moser, C. Eichler, A. Wallraff, A. Isacsson, and A. Bachtold, Nat. Nanotechnol. **12**, 631 (2017).

[52] L. Li, Y. O. Dudin, and A. Kuzmich, Nature (London) **498**, 466 (2013).

[53] A. M. Contreras-Reyes, R. Guérout, Paulo A. Maia Neto, D. A. R. Dalvit, A. Lambrecht, and S. Reynaud, Phys. Rev. A **82**, 052517 (2010).

[54] D. Barredo, V. Lienhard, P. Scholl, S. de Léséleuc, T. Boulier, A. Browaeys, and T. Lahaye, Phys. Rev. Lett. **124**, 023201 (2020).

[55] M. E. Kim, T.-H. Chang, B. M. Fields, C.-A. Chen, and C.-L. Hung, Nat. Commun. **10**, 1647 (2019).

[56] J. D. Thompson, T. G. Tiecke, N. P. de Leon, J. Feist, A. V. Akimov, M. Gullans, A. S. Zibrov, V. Vuletic, and M. D. Lukin, Science **340**, 1202 (2013).

[57] J. de Hond, R. van Bijnen, S. J. J. M. F. Kokkelmans, R. J. C. Spreeuw, H. B. van Linden van den Heuvell, and N. J. van Druten, Phys. Rev. A **98**, 062714 (2018).

[58] K. S. Rajasree, T. Ray, K. Karlsson, J. L. Everett, and S. N. Chormaic, Phys. Rev. Research **2**, 012038(R) (2020).

[59] T. Kazimierczuk, D. Fröhlich, S. Scheel, H. Stolz, and M. Bayer, Nature (London) **514**, 343 (2014).

[60] E. V. Castro, H. Ochoa, M. I. Katsnelson, R. V. Gorbachev, D. C. Elias, K. S. Novoselov, A. K. Geim, and F. Guinea, Phys. Rev. Lett. **105**, 266601 (2010).

[61] C.-H. Chang, N. Rivera, J. D. Joannopoulos, M. Soljacic, and I. Kaminer, ACS Photonics **4**, 3098 (2017).

[62] Y. Yang, A. Massuda, C. Roques-Carmes, S. E. Kooi, T. Christensen, S. G. Johnson, J. D. Joannopoulos, O. D. Miller, I. Kaminer, and M. Soljačić, Nat. Phys. **14**, 894 (2018).